Electronic and optical properties of layered van der Waals heterostructure based on MS_2 (M = Mo, W) monolayers

To cite this article before publication: M. Farkous *et al* 2019 *Mater. Res. Express* in press https://doi.org/10.1088/2053-1591/ab1029

Electronic and optical properties of layered van der Waals heterostructure based on MS_2 (M = Mo, W) monolayers

M. Farkous[1], M. Bikerouin[1], Huong T.T. Phung[2], M. El-Yadri[1], E. Feddi[1,9], F. Dujardin[3], C. A. Duque[4], Do Muoi[5,6], Huynh V. Phuc[7,9], Chuong V. Nguyen[8], Nguyen N. Hieu[7,9]

[1]LaMSci, Group of Optoelectronic of Semiconductors and Nanomaterials, ENSET, Mohammed V University in Rabat, Rabat, Morocco
[2]NTT Hi-Tech Institute, Nguyen Tat Thanh University, Ho Chi Minh City, Viet Nam
[3]Université de Lorraine, LCP-A2MC, 57000 Metz, France
[4]Grupo de Materia Condensada-UdeA, Instituto de Física, Facultad de Ciencias Exactas y Naturales, Universidad de Antioquia UdeA, Calle 70 No. 52-21, Medellín, Colombia
[5]Department of Physics and Engineering Physics, University of Science-VNU.HCM, Ho Chi Minh City, Viet Nam
[6]Department of Natural Sciences, Pham Van Dong University, Quang Ngai, Viet Nam
[7]Institute of Research and Development, Duy Tan University, Da Nang 550000, Viet Nam
[8]Department of Materials Science and Engineering, Le Quy Don Technical University, Ha Noi, Viet Nam
[9]Authors to whom any correspondence should be addressed

E-mail: e.feddi@um5s.net.ma (E. Feddi)

E-mail: hvphuc@dthu.edu.vn (H. V. Phuc)

E-mail: hieunn@duytan.edu.vn (N. N. Hieu)

December 2018

Abstract. In the present work, we investigate the electronic and optical properties of few-layer MS_2 (M = Mo, W) and their van der Waals heterostructure MoS_2/WS_2 using density functional theory. Our calculated results demonstrate that the energy gap of the MS_2 depends tightly on the number of layers. Besides, maximum absorption of the few-layer MS_2 occurs for energies in the range 10 eV to 15 eV and is also highly dependent on the number of layers. While the monolayers MS_2 are direct semiconductors, the MoS_2/WS_2 heterostructure reveals an indirect band gap with a band gap smaller than that of the monolayers MoS_2 and WS_2. In the heterostructure, while the contribution of the W-s orbitals to the conduction band is outstanding, the Mo-s, Mo-p, and W-p orbitals contribute significantly to the valence band. The relocation of the orbital in the monolayers MS_2 to form a heterostructure has brought many interesting properties that can be applied in the transistors based on MoS_2/WS_2 heterostructure.

1. Introduction

Since its discovery in 2004 via mechanical exfoliation [1], graphene attracted much attention from scientists over the past decade with tens of thousands of articles being published.

However, some limitations of this material have been found in the process of using it in technology. For example, because of the zero energy gap, it is difficult to use it in field-effect transistors [2]. In order to get around this technological limitation, scientists have been constantly searching for new two-dimensional (2D) materials that have a graphene-like structure. Thus, many graphene-like structures such as silicene [3], MoS_2 [4], and others [5–7] have been successfully synthesized.

Among these 2D materials, the transition metal dichalcogenides (TMDs) MX_2, where M represents a transition metal and X is a chalcogen atom, are semiconductors with a large natural band gap. The band gap of the TMDs depends not only on M and/or X atoms but also strongly on the number of layers of the material [8, 9]. With natural band gap, the TMD monolayers, such as WS_2, WSe_2, MoS_2, $MoTe_2$, $MoSe_2$, etc... become competing materials for application in nanoelectronics and spintronic devices [10–17]. Physical properties of the TMDs monolayers have been studied by various methods [18–23]. In parallel with consideration of intrinsic properties of two-dimensional materials, van der Waals (vdW) heterostructures offer many possibilities by stacking these 2D layered materials. The vdW heterostructures are predicted to be the current research trend of material scientists [24, 25]. Recently, the fabrication of the vdW heterostructures from TMDs monolayers has been made experimentally [16, 26]. Lopez-Sanchez and co-workers have shown that the TMDs heterostructures can use in photovoltaic and optoelectronic devices because they exhibit very strong light-matter interactions [27]. Besides, many theoretical studies have focused on the electronic properties and the formation of the Schottky barrier in the wdW heterostructures [28–34].

In the present work, we consider the electronic and optical properties of few-layer MS_2 (M = Mo,W) and their heterostructures using the first principles calculations. Our study focuses on the effect of the material thickness (number of layers) on electronic and optical properties of the few-layer MS_2. Electronic properties and charge transfer in the MoS_2/WS_2 heterostructure are also calculated and discussed in details.

2. Details of calculations

In this work, all calculations of the geometric optimization, electronic properties, and optical characters of bulk and few-layer [monolayer (1L), double-layer (2L), and triple-layer (3L)] MS_2 are performed using the FP-LAPW method, which was implemented in the Wien2k simulation package [35]. It is obligatory to test the convergence of numerical parameters, there are two essential parameters which must be refined in order to perfectly describe the systems studied. The first parameter is the product between the muffin-tin radius R_{MT} and the maximum modulus for the reciprocal lattice vectors K_{max} and the second parameter is the number k-point. When we plot these parameters as a function of the total energy we must choose the values where the curve begins to stabilize. The total energy founded at the equilibrium state of MoS_2 bulk was -19392.294 eV. In the interstitial region, the wave function was expanded with the basis function up to $R_{MT}K_{max} = 7$. The charge density is implemented from Fourier series up to $G_{max} = 12$. To avoid the overlapping

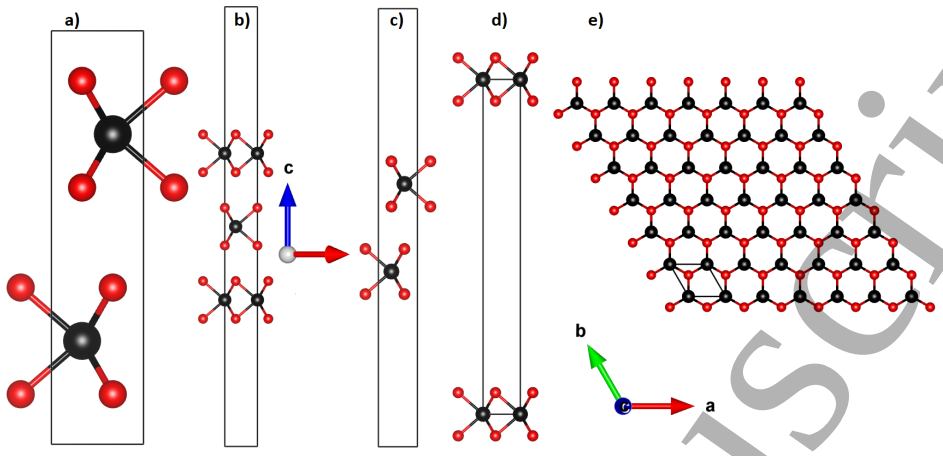

Figure 1. The atomic structure of the MS_2 (M=Mo, W) bulk (a), trilayer (b), bilayer (c), and monolayer (d). (e) Top view of the MS_2 monolayer. The black and red balls represent the atoms of metal M and sulphur S, respectively.

between atomic spheres, the R_{MT} were chosen. In this work, we use the generalized gradient approximation (GGA) based on Perdew-BurkeErnzerhof (PBE) parameterization and local density approximation (LDA) for MS_2 (M = Mo, W) multilayers (1L, 2L, 3L, and bulk). In addition, the modified Becke and Johnson (MBJ) approximation was also used for the bulk MS_2. The geometric optimization was carried out with respect to both the atomic coordinates and the lattice constants, using the PORT minimization method. The k-mesh of $16 \times 16 \times 3$ and $14 \times 14 \times 1$ of the irreducible Brillouin zone (BZ) were used for bulk MS_2 (M = Mo, W) and their layers, respectively.

3. Results and discussion

3.1. Structural parameters

The TMD MS_2 (M = Mo, W) has a hexagonal structure consisting of S–M–S layers as shown in Fig. 1. The units cells of bulk MS_2 belongs to the space group $P63/mmc$ and contains six atoms (two M atoms and four S atoms). The metal atoms (M) of one layer are directly above the S atoms of the other layer and vice-versa. The MS_2 monolayer is shown in Fig. 1(d,e).

Our computed results for the structural parameters of the optimized bulk MS_2 structures using GGA and LDA approximations are listed in Tab. 1. Our results are in good agreement with available experimental data [36, 37] and theoretical calculations [18, 38–42].

3.2. Electronic properties

In Fig. 2, we illustrate the band structure of the few-layer MS_2 with the spin-orbit coupling (SOC) and without spin-orbit coupling (nSOC) using PBE, LDA, and MBJ approximations. The MBJ approximation is used only for the bulk cases. We can see that the bulk and few-layer 2H-MS_2 (M = Mo, W) are semiconductors with indirect band gap, forming between the

Table 1. Calculated lattice parameters a and c and the M–S bond length d_{M-S} of bulk MS_2 (M = Mo, W) using different functionals

	LDA		PBE	
	MoS_2	WS_2	MoS_2	WS_2
a (Å)	3.141	3.14	3.186	3.184
	3.139 [39]	3.136 [39]	3.194 [39]	3.194 [39]
c (Å)	12.22	12.27	12.40	12.44
	12.182 [39]	12.375 [39]	12.435 [39]	12.640 [39]
d_{M-S} (Å)	2.40	2.395	2.43	2.428
	2.39 [40]	2.39 [38]	2.42 [38]	2.42 [38]

lowest unfilled state of the conduction band (LOMO) in the K–Γ path and the highest filled state of the valence band (HOMO) at the Γ point. However, when bulk MS_2 are transformed into monolayer form, it can be seen that a transition from the indirect to a direct band gap was observed. It indicates that the MS_2 (M = Mo, W) monolayers are semiconductors with the direct band gaps, forming between the HOMO and LOMO at the K point.

The direct gap in MS_2 depends on the localized d-orbital of the transition metal atoms M, located in the middle of the S–M–S sandwiches, that justify when the number of layers is decreased the state of the K-point remains almost constant. While the nature of an indirect band gap in these materials depends on the overlap of d-orbital of transition metal atoms and the p-orbital of the chalcogenide atoms, which depends strongly on the interlayer coupling. Thus, as the number of layers is decreased the intrinsic direct band gap of the material becomes more pronounced. This justifies the reduction of energy states between K and Γ when the number of layers is decreased. Also, the transform from the indirect gap in bulk material to the direct gap in the monolayer is due to the quantum confinement of charge carriers. It is also observed that, at the valence band edge at the K point, the band structure splits into two/three bands for bilayer/trilayer MS_2 due to the interlayer hopping, which leads to the band structure modification significantly.

The calculated band gap for the MS_2 are listed in Tab. 2. Our DFT calculated results for energy gaps are close to the results of previous experiment measurements [36, 37] and theoretical studies [18, 38, 39, 41, 42]. Minor differences between our results and previous results in the case of trilayer MS_2 are due to the stacking configurations, forming between three different MS_2 monolayers. It is clear that for the 2D MS_2 trilayer, there are many different stacking configurations, forming between three different MS_2 monolayers, such as AAA, AAB, ABA, ABB stacking and so on. The electronic properties, including the band gap of MS_2 trilayer, depend strongly on their stacking configurations. In this work, we focus on the ABA stacking configuration of the MS_2 trilayer. This finding was observed in 2D MS_2 trilayer [43]. Also, our results are in good agreement with a previous theoretical report (about 1.17 eV for MoS_2 trilayer) [44]. The dependence of the energy gap on the number of layers (thickness) of the MS_2 is also shown in Fig. 3. As shown in Fig. 3, the band gap of the MS_2 decreases because of the SOC effect. Besides, when the SOC effect is included, as shown

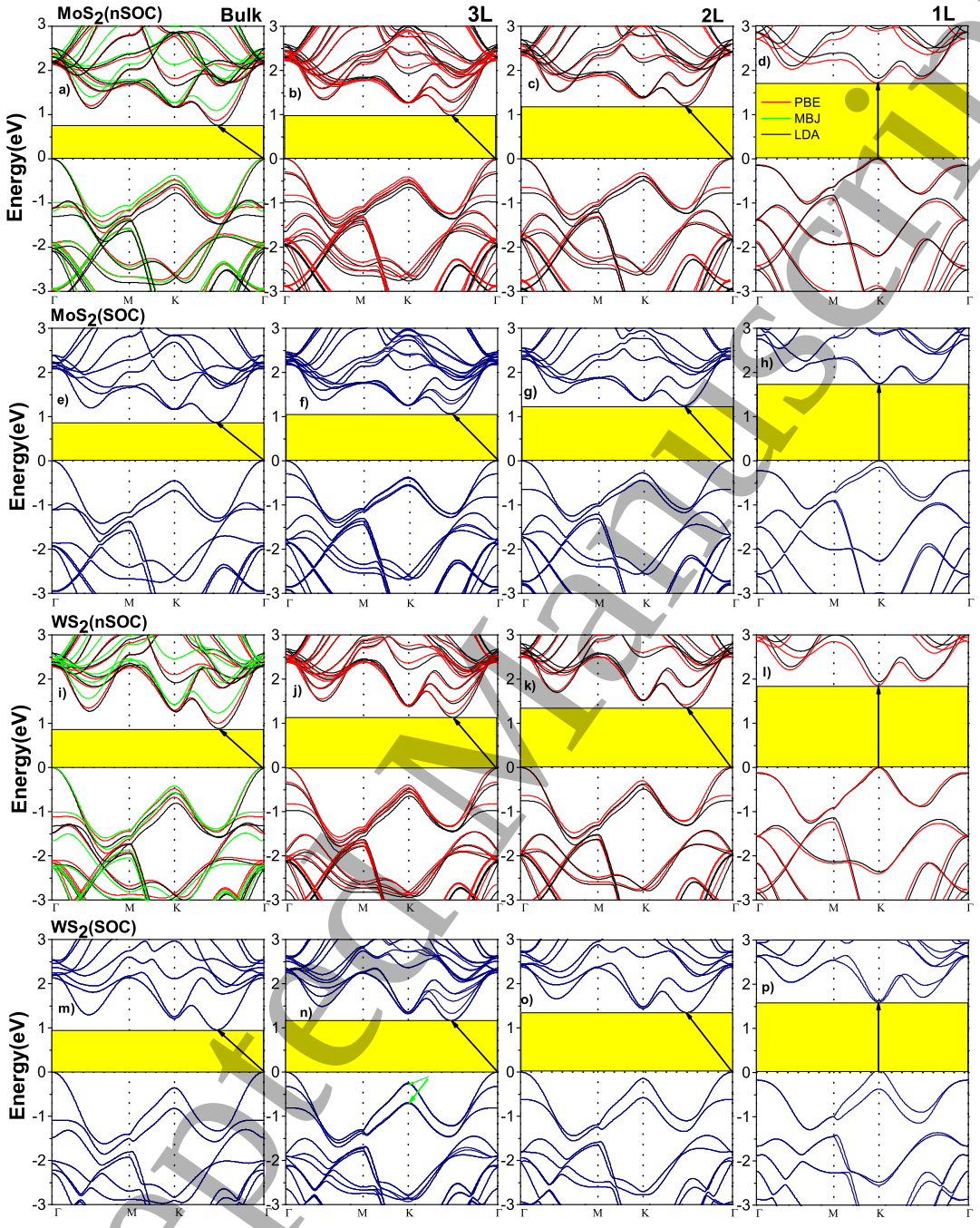

Figure 2. Band structures of (MoS_2 and WS_2) bulk, trilayer (3L), bilayer (2L), and monolayer (1L) are shown in (a-d) and (i-l), respectively. nSOC and SOC stand for without and with spin-orbit coupling, respectively.

in Fig. 2(e-h, m-p), the splitting pattern is strongly changed. The valence band edges split into two degenerate manifolds. Similar to MoS_2, the WS_2 has the same properties, except the valence band splitting at K point, are much greater than that of MoS_2. The different value of splitting spin-orbit ΔSOC are grouped in the Tab. 3. Our results are in good agreement with the previous works [45–50].

Figure 4 shows the partial density of states (PDOS) of the few-layer MS_2 (Mo, W). It

Table 2. Calculated band gap of few-layer MS_2 (M = Mo, W) using LDA and PBE functional with and without spin orbit coupling (SOC).

	MoS_2				WS_2			
Functionals	1L	2L	3L	Bulk	1L	2L	3L	Bulk
LDA	1.83	1.23	1.03	0.83	1.94	1.40	1.18	0.941
LDA(SOC)	1.75	1.22	1.02	-	-	-	-	-
PBE	1.72	1.29	1.11	0.93	1.85	1.45	1.26	1.04
PBE(SOC)	1.65	1.28	1.09	0.90	1.65	1.38	1.20	1.00
MBJ	-	-	-	1.14	-	-	-	1.27
PBE [18, 38, 39, 41, 42]	1.67, 1.73	1.23	-	-	1.81	-	-	-
LDA [18, 38, 39, 41, 42]	1.84	1.19	-	0.76	-	-	-	
Exp. [36, 37]	1.84, 1.87	-	-	1.23	1.96	-	-	1.3

Table 3. ΔSOC splitting the valence band at K-point in the bulk, trilayer (3L), bilayer (2L), and monolayer (1L) MS_2 from first-principles calculations.

	ΔSOC (meV)			
	1L	2L	3L	Bulk
MoS_2	147	169	176	220
	147 [45], 145 ± 4 [46]	-	-	196 ± 22 [47]
WS_2	430	435	437	467
	430 [48], 400 [49]	430 [50]	430 [50]	450 [49], 466 [47]

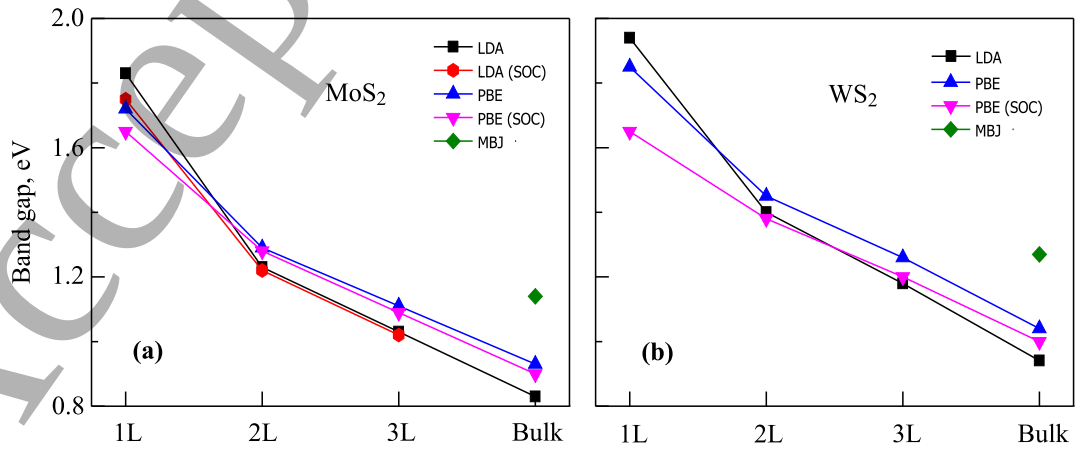

Figure 3. Dependence of band gap of MoS_2 (a) and WS_2 (b) on the number of layers (L).

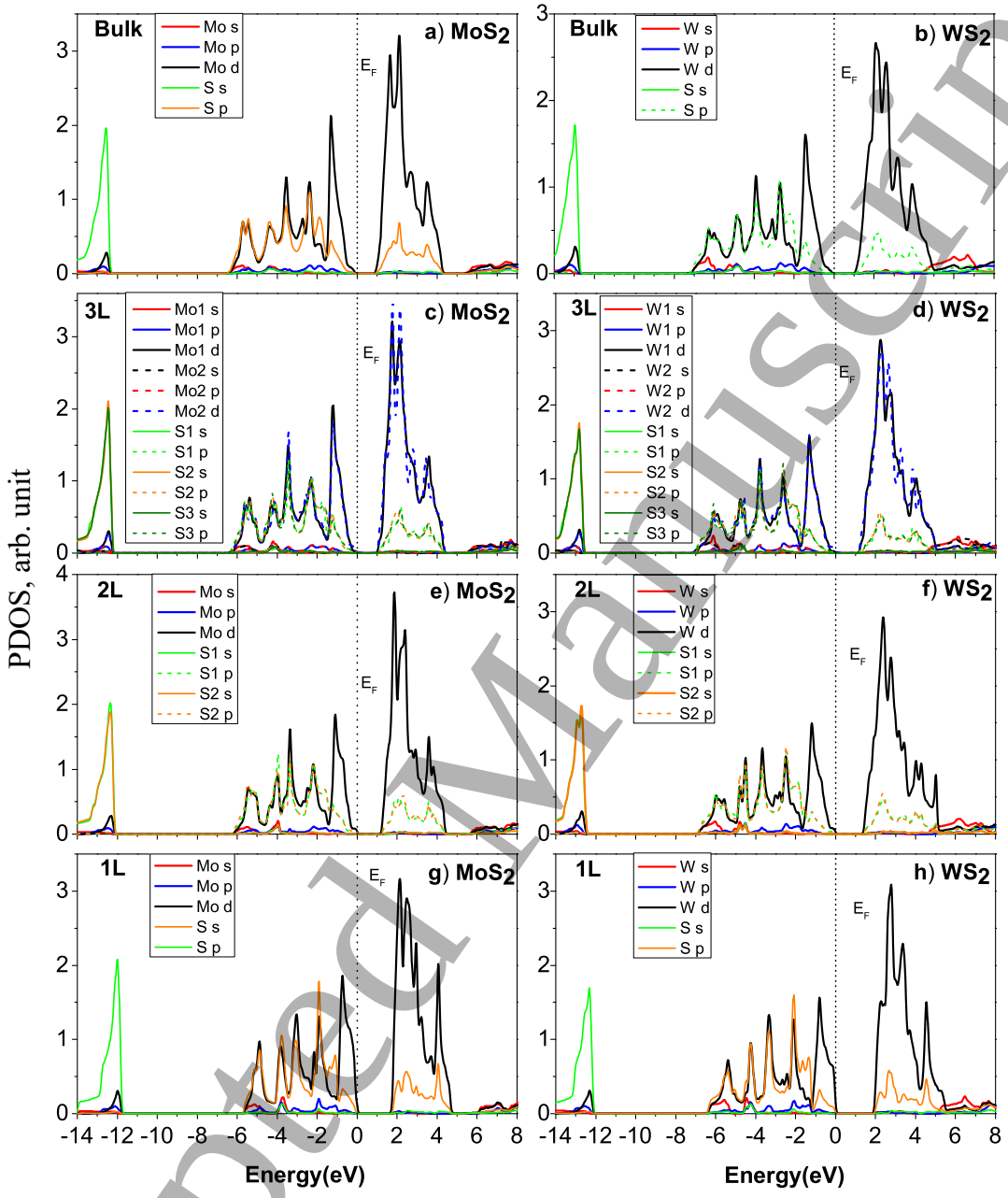

Figure 4. Partial density of states (PDOS) for (MoS_2 and WS_2) bulk (a, b), trilayer (3L) (c,d), bilayer (2L) (e,f) and monolayer (1L) (g,h), respectively.

is seen that the DOS of MoS_2 and WS_2 are similar. The bands around -14 eV are mainly contributed from the $3s$-S orbital. The band near the Fermi level are mainly contributed from the d-Mo/W and p-S orbitals.

3.3. Optical properties

Since the number of layers strongly affects the physical properties of MS_2 (with M = Mo, W), it is natural to expect that it also gives a vital effect on the optical properties. To

study the optical properties, we use the dielectric function $\varepsilon(\omega) = \varepsilon_1(\omega) + i\varepsilon_2(\omega)$, where $\varepsilon_1(\omega)$ and $\varepsilon_2(\omega)$ are respectively its real and imaginary parts, ω being the photon energy. The imaginary part can be obtained theoretically from the calculations of momentum matrix elements between the occupied and unoccupied states as follows [51]

$$\varepsilon_2(\omega) = \frac{e^2\hbar}{\pi m^2\omega^2} \sum_{v,c} \int_{BZ} |\langle U_{ck}|e\nabla|U_{vk}\rangle|^2 \delta\{\omega_{ck}(k) - \omega\} d^3k, \quad (1)$$

while the real part has been calculated from the imaginary part via the Kramers Kronig relation

$$\varepsilon_1(\omega) = 1 + \frac{2}{\pi} \int_1^{\omega} \frac{\omega_1 \varepsilon_2(\omega_1) d\omega_1}{\omega_1^2 - \omega^2}. \quad (2)$$

For the compounds having hexagonal symmetry, the dielectric properties experiments has been performed with the electric field $\vec{E}$ perpendicular or parallel to the crystallographic

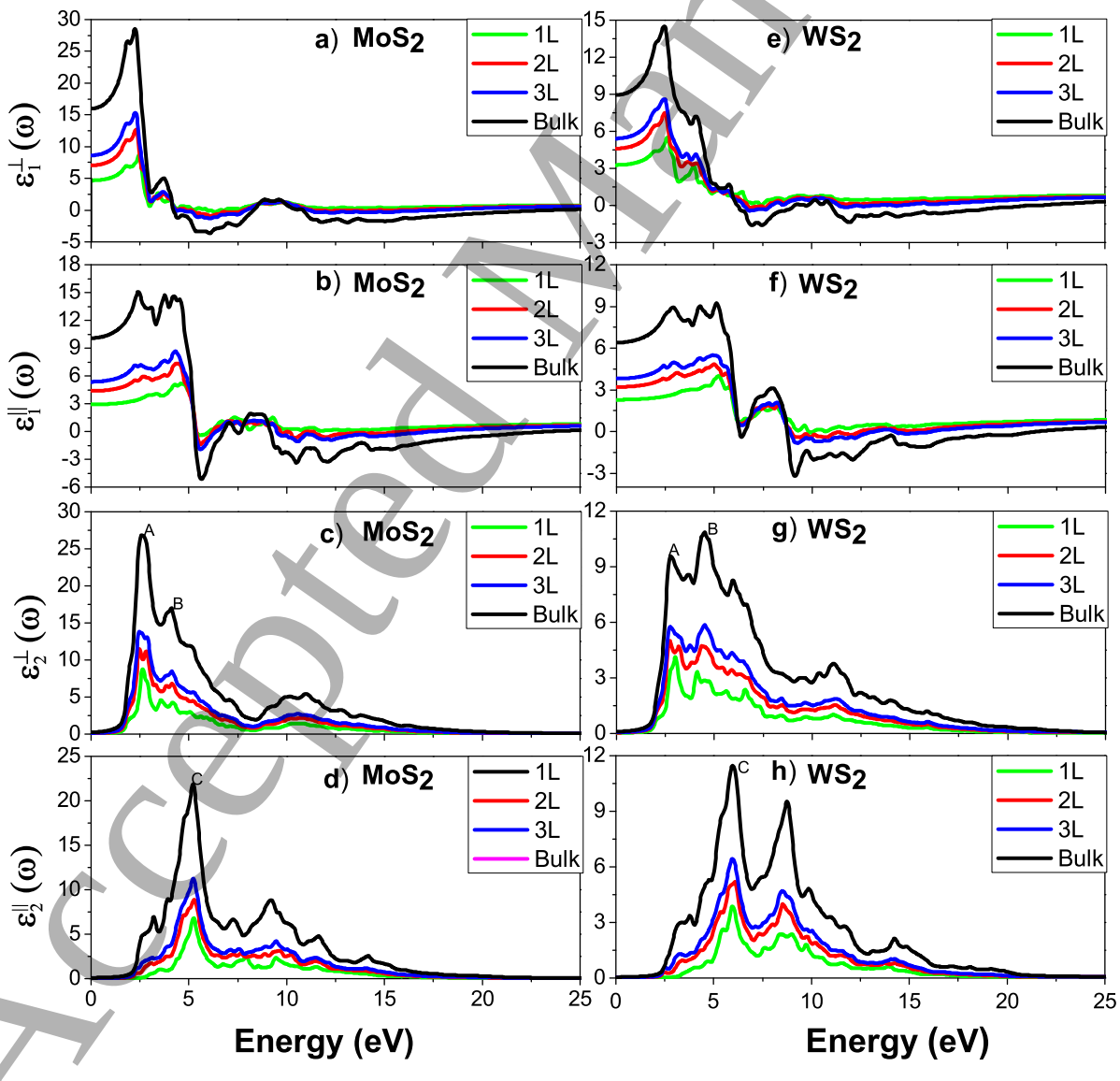

Figure 5. Calculation of the real and the imaginary parts of the dielectric function of MoS_2 (a–d) and WS_2 (e–h).

Table 4. The optical properties of MS_2 (Mo, W) bulk, trilayer (3L), bilayer (2L), monolayer (1L). The peaks A, B, and C are shown in Fig. 5. Only dielectric function ε at 0 eV and the dichroic ratio $\Re$ at 2 eV and 15 eV are shown.

	1L		2L		3L		bulk	
	MoS_2	WS_2	MoS_2	WS_2	MoS_2	WS_2	MoS_2	WS_2
Peak A	2.65	3.0	2.5	2.74	2.5	2.74	2.6	278
Peak B	3.6	4.12	4.1	4.4	4.1	4.5	4.1	4.5
Peak C	4.1	4.7	5.3	6.0	5.25	5.9	5.2	5.9
$\varepsilon_1^{\perp}(0)$	4.6	3.27	7.05	4.61	8.62	5.42	15.97	8.21
$\varepsilon_1^{\parallel}(0)$	2.9	2.28	4.36	3.20	5.36	3.80	10.08	6.39
$\varepsilon_r(0)$	4.16	2.98	6.28	4.19	7.69	4.94	14.28	8.18
$\Re$(2 eV)	0.955	0.935	0.91	0.88	0.894	0.84	0.892	0.81
$\Re$(15 eV)	0.17	0.059	0.11	0.06	0.09	0.057	0.03	0.11

direction, renamed c-axis [52]. The measured dielectric functions $\varepsilon^{\parallel}$ and $\varepsilon^{\perp}$ are given by [52]

$$\varepsilon^{\perp}(\omega) = \frac{1}{2}[\varepsilon^{xx}(\omega) + \varepsilon^{yy}(\omega)], \tag{3}$$

$$\varepsilon^{\parallel}(\omega) = \varepsilon^{zz}(\omega). \tag{4}$$

In Eqs. 3 and 4, $\varepsilon^{xx}(\omega)$, $\varepsilon^{yy}(\omega)$, and $\varepsilon^{zz}(\omega)$ are the diagonal parts of the dielectric matrix $\varepsilon^{ij}(\omega)$. Then the expression for the absorption coefficient $\alpha(\omega)$, the refraction index $n(\omega)$, and the extinction coefficient $k(\omega)$ can be gained by $\varepsilon_1(\omega)$ and $\varepsilon_2(\omega)$ [53]

$$\alpha(\omega) = \sqrt{2\omega}\left[\sqrt{\varepsilon_1^2(\omega) + \varepsilon_2^2(\omega)} - \varepsilon_1(\omega)\right]^{1/2}, \tag{5}$$

$$n(\omega) = \frac{1}{\sqrt{2}}\left[\sqrt{\varepsilon_1^2(\omega) + \varepsilon_2^2(\omega)} + \varepsilon_1(\omega)\right]^{1/2}, \tag{6}$$

$$k(\omega) = \frac{1}{\sqrt{2}}\left[\sqrt{\varepsilon_1^2(\omega) + \varepsilon_2^2(\omega)} - \varepsilon_1(\omega)\right]^{1/2}. \tag{7}$$

Figure 5 shows the $\varepsilon_1(\omega)$ and $\varepsilon_2(\omega)$ of MoS_2 and WS_2 from bulk to thin film. The $\varepsilon_2(\omega)$ part shows a structure with peaks A, B and C, and the corresponding energies are listed in Tab. 4. Our results on $\varepsilon_2(\omega)$ are found to be in very good agreement with the theoretical calculations by Reshak [52]. In the energy range from 2 eV to 5 eV, all the intense peaks show a similar trend, with the exception of their energy values. Almost all the perpendicular components of $\varepsilon_2(\omega)$, hereinafter referred as $\varepsilon_2^{\perp}(\omega)$, show two intense peaks located around 2.3 and 4.2 eV, which is due to transition directly between the S-p (maximum valence band) states and the Metal M-d (minimal conduction band) respectively at points Γ and M. Interestingly, in the parallel component of $\varepsilon_1^{\perp}(\omega)$, $\varepsilon_1^{\parallel}(\omega)$, intense peaks are observed in the range from 4.5 eV to 6 eV. The different peaks have been grouped in the Tab. 4 (denoted by peaks A, B, and C).

Figure 5 (a,b,e,f) shows the calculated results of the $\varepsilon_1(\omega)$ part of the dielectric function. The obtained dielectric spectra for the different number layers are similar to each other,

showing a very weak influence of the low-inter-layer bond in the range of high energies. The real part can be negative in some values of energy. Focusing on the $\varepsilon_1^{\perp}(\omega)$ in MoS_2 [Fig. 5(a)] and WS_2 [Fig. 5(e)], we see that there are maximum peaks in the $\varepsilon_1^{\perp}(\omega)$ at low energy region. These peaks tend to shift toward the lower energy region as we increase the number of layers of the material. Here, the most important quantity is the zero energy limit of the dielectricity, that is, the static dielectric constant for the $E \perp c$ and $E \| c$ polarization, which are summarized in Tab. 4. We see that for the case of the bilayer, the dielectric constants decreases down to 55% compared with MoS_2 and WS_2 bulks. When the number of layers increases, the real part increases. In the case of three layers, the difference between the dielectric constants of the bulk and that of the three layers is reduced to 45%. This gives the possibility of storing more electrical potential energy. Starting from MoS_2 bilayer, the ultrathin are classified as high dielectric constant materials [54] ($\varepsilon_1^{\|}(0) > 7$) and they are considered as interesting material for application in nanoelectronic devices [54].

It is well-known that the dielectric functions of the WS_2 are similar to that of the MoS_2

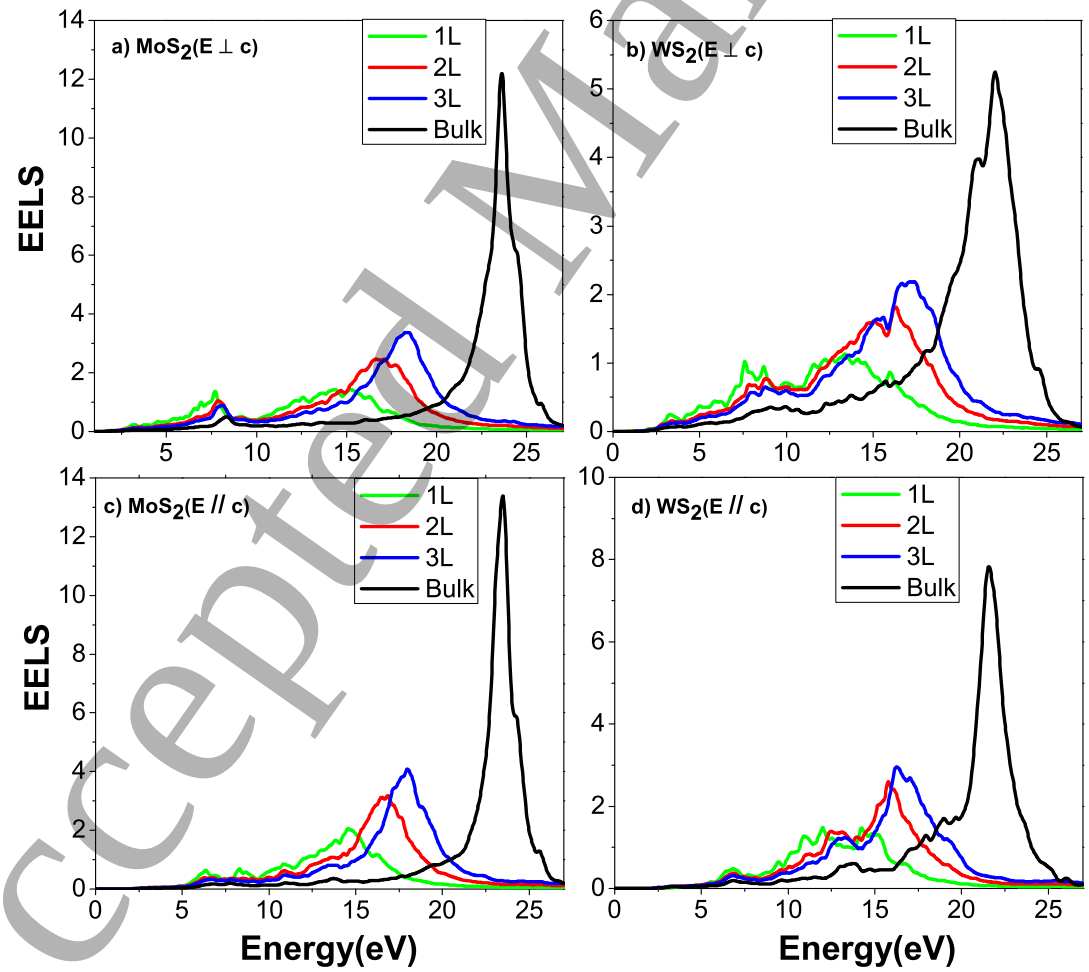

Figure 6. Variation of Electron energy loss spectra (EELS) of MS_2 for electric vector perpendicular to c-axis ($E \perp c$) and electric vector parallel to c-axis (($E \| c$)), with number of layers.

in the range from 0 to 4 eV. Our calculations are in good agreement with the experimental data [55], except for the excitonic peak at 1.9 eV for the bulk MoS_2.

The electron energy loss spectra (EELS) for the parallel and perpendicular polarization, describing the loss of energy of a fast electron passing through the material, can be defined as follows [53]

$$I_m\left\{\frac{-1}{\varepsilon(\omega)}\right\} = \frac{\varepsilon_2(\omega)}{\varepsilon_1^2(\omega)+\varepsilon_2^2(\omega)}. \tag{8}$$

The characteristics of loss energy appearing at energies lower than 50 eV, although contain a wealthy information, are less studied. In this region, some of the energy loss processes taking place are the collective excitations of the valence electrons. This phenomenon could be investigated as a plasma. The excitations can appear when the incident electron interferes with the outer valence electrons, causing collective oscillations which are called plasmons at frequency ω_p.

Fig. 6 (a,b) show that the energy loss spectra of electrons consist of two important resonance characteristics for perpendicular polarization ($E \perp c$). The plasmons peak π below 10 eV is due to the collective $\pi - \pi^*$ transition while the plasmons peak π–σ above 10 eV results from the σ–σ^* excitation. The electron energy loss spectra for parallel polarization ($E \parallel c$) of MS_2 [see Fig. 6(c-d)] consists of one prominent resonance feature above 10 eV [56] due to π-σ plasmons excitation. We can see a remarkable shift in the plasmon peaks energies π and π–σ for parallel and perpendicular polarization is the result of the limit from bulk to the monolayer. It appears that when we go from bulk to monolayer, the electron average concentration decreases, resulting from a considerable increase in the electron effective mass. Therefore, the lowest value of resonant frequency for monolayer is consistent with the plasmon frequency described by the equation

$$\omega_p = \frac{Ne^2}{\varepsilon_0 m_{eff}}. \tag{9}$$

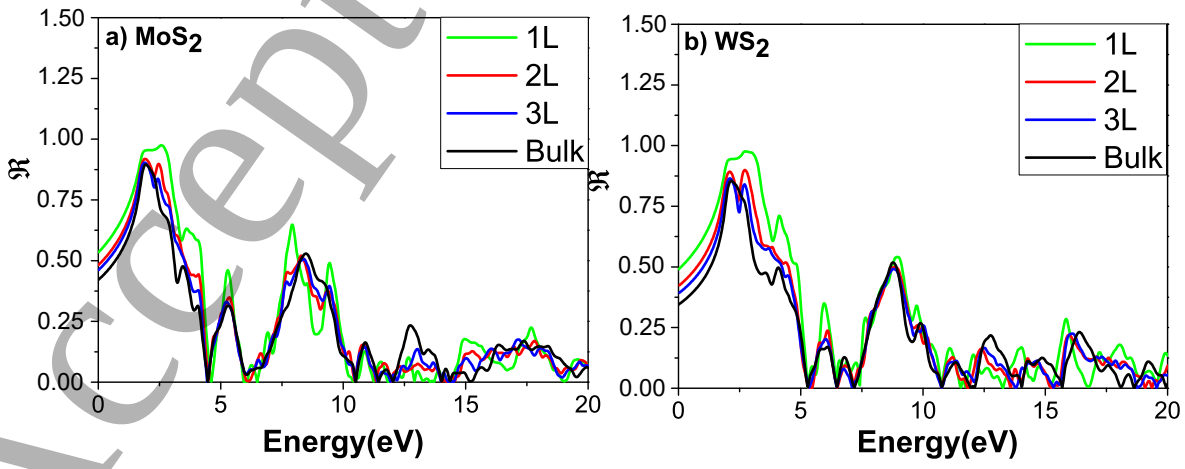

Figure 7. Dependence of the degree of anisotropy the number of layers in (a) MoS_2 and (b) WS_2.

Figure 6 shows the variation of plasmon peak's intensity with the number of layers. It can be seen that the π–σ plasmon peak's intensity increases while the π plasmon peak one decreases with the increase of the number of layers from the monolayer to bulk. To quantify the degree of anisotropy in the MoS_2 and WS_2 from bulk state to the thin film, the dichroic ratio $\Re$ at different energies was calculated using the following relationship

$$\Re = \left| \frac{\varepsilon_2^{\perp}(\omega) - \varepsilon_2^{\parallel}(\omega)}{\varepsilon_2^{\perp}(\omega) + \varepsilon_2^{\parallel}(\omega)} \right|. \tag{10}$$

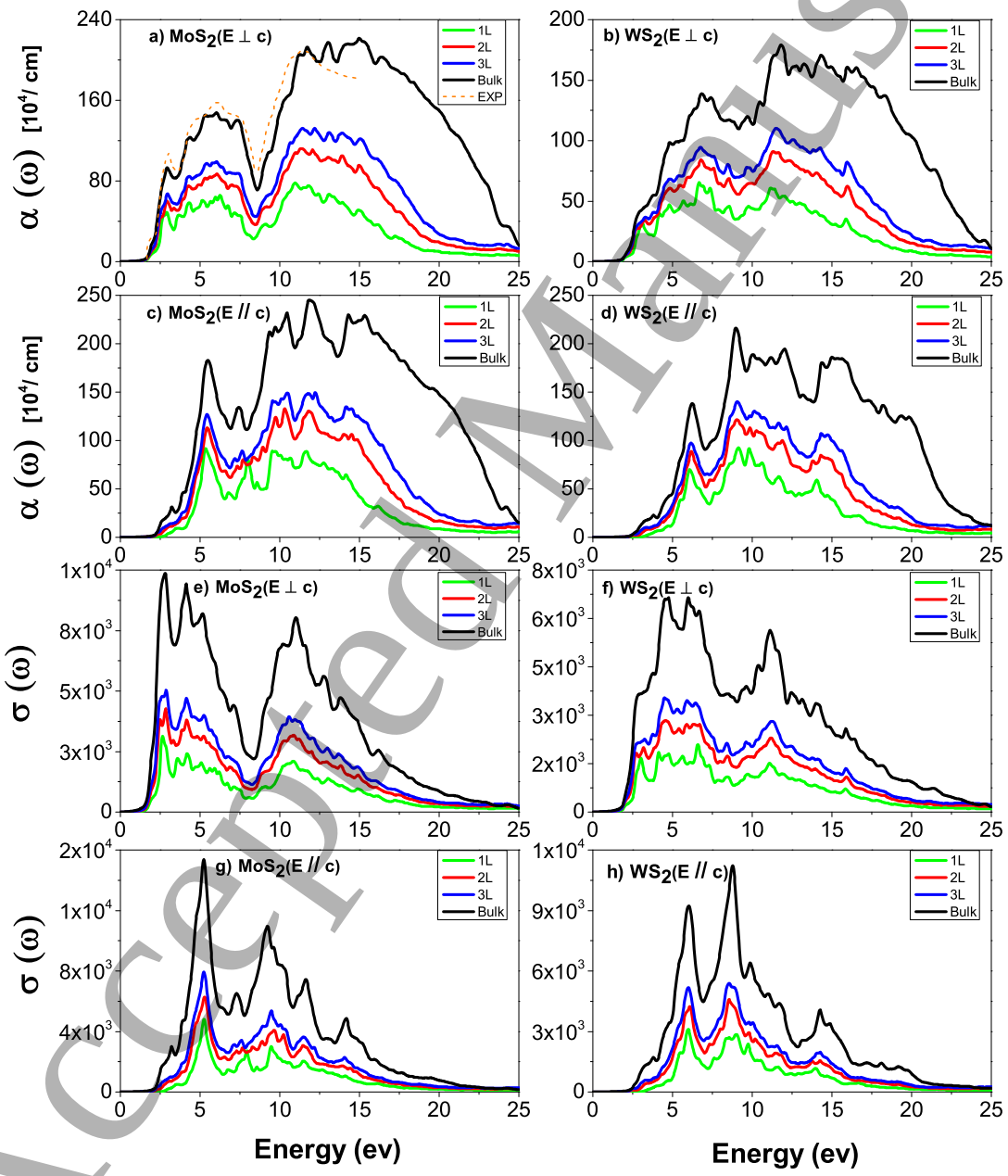

Figure 8. Variation of the absorption $\alpha(\omega)$ (a-d) and the conductivity $\sigma(\omega)$ (e-f) for the polarizations ($E \perp c$, $E \| c$) with the variation of layers number. The dotted line in a) shows the experimental data for the polarization $E \perp c$ perpendicular to c-axis.

Table 5. Refractive index $n^{\perp,\parallel}(0)$ and the birefringence $\Delta_n(0)$ at zero energy of the bulk, trilayer (3L), bilayer (2L), and monolayer (1L) MS_2 (M = Mo, W).

	1L		2L		3L		Bulk	
	MoS_2	WS_2	MoS_2	WS_2	MoS_2	WS_2	MoS_2	WS_2
$\Delta_n(0)$	0.45	0.3	0.565	0.36	0.62	0.38	0.82	0.46
	0.3 [62]		0.57 [62]				0.79 [62]	
$n^{\perp}(0)$	2.16	1.8	2.65	2.14	2.93	2.32	3.99	2.99
$n^{\parallel}(0)$	1.7	1.51	2.08	1.78	2.31	1.95	3.17	2.52

Our calculations show that, in the low energy range (< 9 eV), the dielectric functions are strongly anisotropic and they become isotropic in the higher energy range as shown in Fig. 7. We also note in the figure that the anisotropy of MoS_2 and WS_2 increases by reducing the layer number from bulk form to monolayer. Therefore, the MS_2 monolayer has a strong anisotropic compared to the thicker leather. It is well-known that TMDs are assumed to be optically isotropic material. However, several theoretical works indicated that the 2D MoS2 shows high anisotropic physical properties, which can be related to the layered structure because of the strong covalent bonding of atoms in the same layer and the weak interlayer interactions [57]. On the other hand, the anisotropic effects are found to be considerable in monolayer MoS_2 [58] and Molina and co-workers [59] previously demonstrated that the dielectric functions of MoS_2 monolayer are strong anisotropy. This makes MS_2 becoming a potential candidate for applications in optoelectronic devices.

The measurement of the penetration of the photon in the material before its absorption can be described by the absorption coefficient $\alpha(\omega)$. Figure 8 shows the absorption coefficient and the conductivity $\sigma(\omega)$ of MoS_2 and WS_2 from bulk to a thin film for a polarization perpendicular and parallel to the c-axis. The absorption coefficients of MS_2 bulk and few-layers are similar to the imaginary dielectric functions in the region from 0 to 3.5 eV, which corresponds directly to the electronic transitions, and it is clear that the MS_2 monolayer shows a minimal absorption increases as we increase the layer number. Figure 8 also shows a strong decreasing of the absorption coefficient before 2.2 eV, which indicates that a photodetector using MS_2 is only useful for detecting the light above 2.2 eV. In the case of MoS_2 layered material, it has shown excellent characteristics for application as an ultraviolet detector [60, 61].

Figure 9 (a-b, e-h) shows the refractive index and the extinction coefficient of MS_2 monolayer and multilayer, respectively. It can be seen from the figure that when the number of layers reduces from bulk to monolayer, the maximum peaks of the refractive index move to the higher energy region while those of the extinction coefficient gives a red-shift. We also note that the maximum peak's amplitude of the MS_2 bulk is higher than that of the layers. Therefore, the amplitude increases by increasing of thin film thickness, which means that the bulk material absorbs the light better than the thin films. Our calculated results is in good agreement with a previous work [62].

From Tab. 5, we can see that the static refractive index ($n^{\perp}(0)$, $n^{\parallel}(0)$) in the perpendicular

and parallel directions of the electric field is equal to the square root of the component real static dielectric $\varepsilon_1^{\perp}(0)$ and $\varepsilon_1^{\parallel}(0)$, i.e.

$$n^{\perp}(0) = \sqrt{\varepsilon_1^{\perp}(0)}, \tag{11}$$

$$n^{\parallel}(0) = \sqrt{\varepsilon_1^{\parallel}(0)}. \tag{12}$$

Figure 10 depicts the variation of birefringence $\Delta_n(\omega)$ in MoS_2 with photon energy for bulk and the different number of layers. In solid MoS_2, it is found that $\Delta_n(0)$ is 0.82, which is significantly higher than that obtained from a thin film of 2L (0.565). The monolayer shows

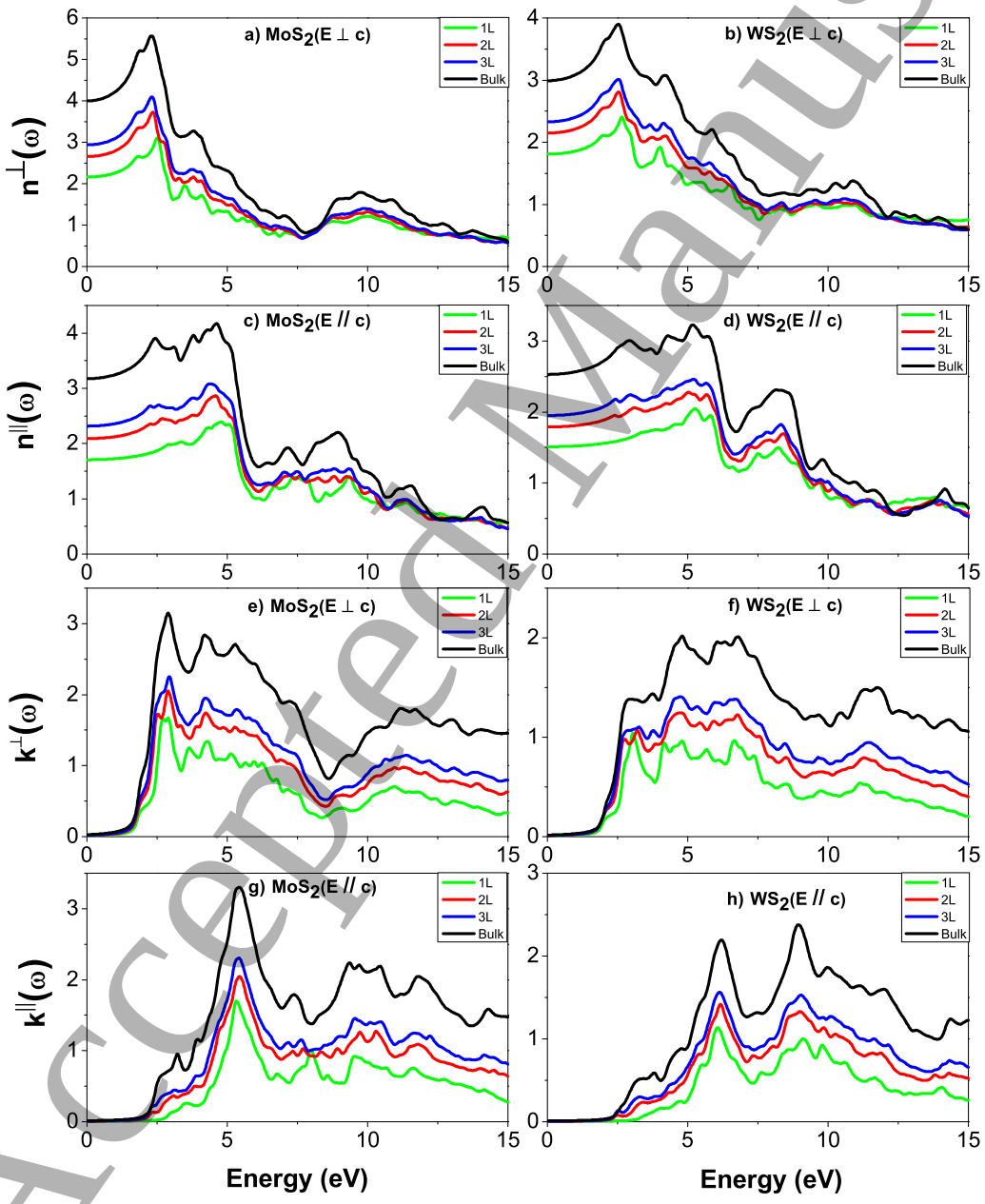

Figure 9. Variation of the the refractive index $n(\omega)$ (a-d) and the extinction coefficient $k(\omega)$ (e-f) for the polarizations ($E \perp c$, $E \| c$) with the variation of layers number.

the lowest value (0.45) of $\Delta_n(0)$. Besides, by increasing the number of layers, the $\Delta_n(\omega)$ also increases and reaches the maximum for the bulk. The highest value of $\Delta_n(\omega)$ is found at around 2.2 eV of energy for most layers, which is close to the direct bandgap for layers at Γ. For lower energy, the birefringence $\Delta_n(\omega)$ is positive. However, in the higher energy region, the opposite trend is observed where the $\Delta_n(\omega)$ becomes negative. We have observed that at a critical value of 3 eV (called isotropic point) the $\Delta_n(\omega)$ tends to zero. The experimental birefringence of rhenium disulfide was addressed in Refs. [63, 64] where the phenomenon occurs due to anisotropic confinement in the crystal structure. For molybdenum disulfide, the birefringence was obtained in the liquid crystal form [65]. In the monolayer configuration, it has been difficult to measure and only reports of measuring the complex refractive index exist [66]. It is hoped that soon this controversy is cleared up in the literature.

3.4. MoS_2/WS_2 van der Waals heterostructure

In this part, we consider the electronic and optical properties of the vdW heterostructure MoS_2/WS_2 composed by the vertical stacking of two different monolayers MoS_2 and WS_2. The optoelectronic behavior of this vdW heterostructure is still unclear at the nanoscale limit. In particular, it is experimentally unknown whether the optical transitions will be indirect or direct in this heterobilayer.

Each layer of MS_2 (M = Mo or W) is composed of a plane of Mo/W atoms sandwiched between two planes of S atoms as shown in Fig. 11. Hybrid layers are maintained by weak vdW forces. Band structures of the monolayers MS_2 and the vdW heterostructure MoS_2/WS_2 are shown in Fig. 12. Figure 12(a,b) shows that the monolayers MoS_2 and WS_2 are the direct bandgap semiconductors, while Figure 12(c) reveals that the MoS_2/WS_2 heterostructure is a semiconductor with an indirect gap of 1.46 eV formed from the valence band maximum (VBM) at the point Γ and the conduction band minimum (CBM) at the K point. Our calculated results are consistent with the available experimental measurements [16] and theoretical reports [67, 68]. The PDOS of the MoS_2/WS_2 heterostructure is also shown in

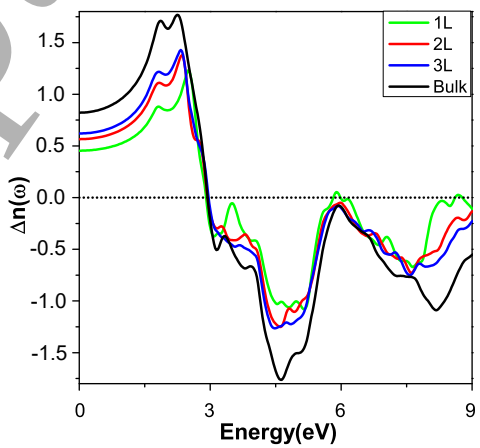

Figure 10. The variation of birefringence in MoS_2 with photon energy for bulk and different number of layers.

Fig. 13.

From the band structure and the DOS of the MoS_2/WS_2 heterostructure, we can see that the CBM locating at the K-point is due to states d of the Mo atoms, while the VBM locating at the Γ-point is due to states d of the W atoms. Since the VBM and CBM can be located on different semiconductors [type II alignment as illustrated in Fig. 11(b)], the MoS_2 monolayer is the barrier material for the holes whereas the monolayer WS_2 acts as a barrier material for electrons.

An important consequence of the vdW stacking of these layers is the absence of a depletion region which causes rapid interlayer charge transfer [26, 69]. Thereafter, charge carriers are largely localized in opposite layers, the 2D heterojunction manifests a vertical p-n junction [70, 71]. In then MoS_2/WS_2 hetero-bilayers, electrons are confined to the MoS2 layer and holes are confined to the WS_2 layer. Hong and co-workers have investigated the ultrafast charge transfer in MoS_2/WS_2 heterojunction and they found the charge-transfer time is in femtosecond scale, very smaller than that in MS_2 (M=Mo, W) monolayer [26]. The investigated MoS_2/WS_2 heterostructure exhibits a lower energy gap than the bands of each of the two distinct monolayers, which can be advantageous by separating electron-hole pairs. This character is useful for the detection and harvesting of light. The vertical separation of the electron and the hole will eliminate the recombination of electron-hole pairs and prolong the lifetimes ($\sim$ 40 ns [72]) of interlayer excitons compared to intralayer in the MS_2 monolayers. This long lifetime is important because it circumvents the limitation imposed by the picosecond lifetime of the excitons in MS_2 monolayers.

In the Fig. 14, we have plotted the dielectric constant $\varepsilon(\omega)$ and the refractive index $n(\omega)$

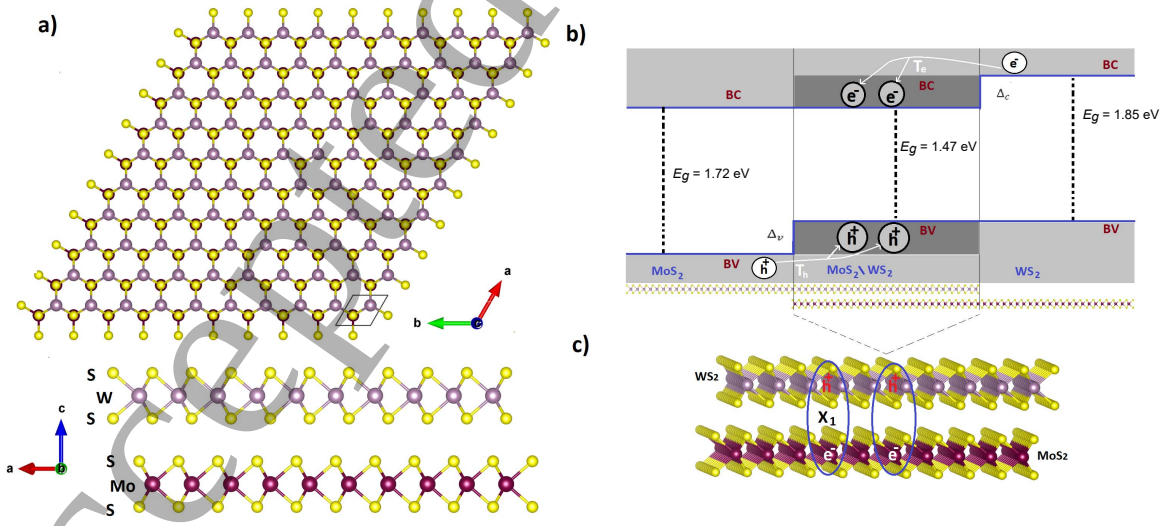

Figure 11. (a) The atomic structure of the heterostructure MoS_2/WS_2. (b) Energy-level diagram showing type-II band alignment and interlayer charge transfer in the MoS_2/WS_2 heterostructure. $T_e(T_h)$ represents the interlayer charge transfer rate for electrons (holes). $\triangle_c$ ($\triangle_v$) is the conduction (valence) band offset between the two monolayers. (c) Illustration of the interlayer excitons formed from the large electron–hole Coulomb interaction spatially separated in different layers of the heterobilayer.

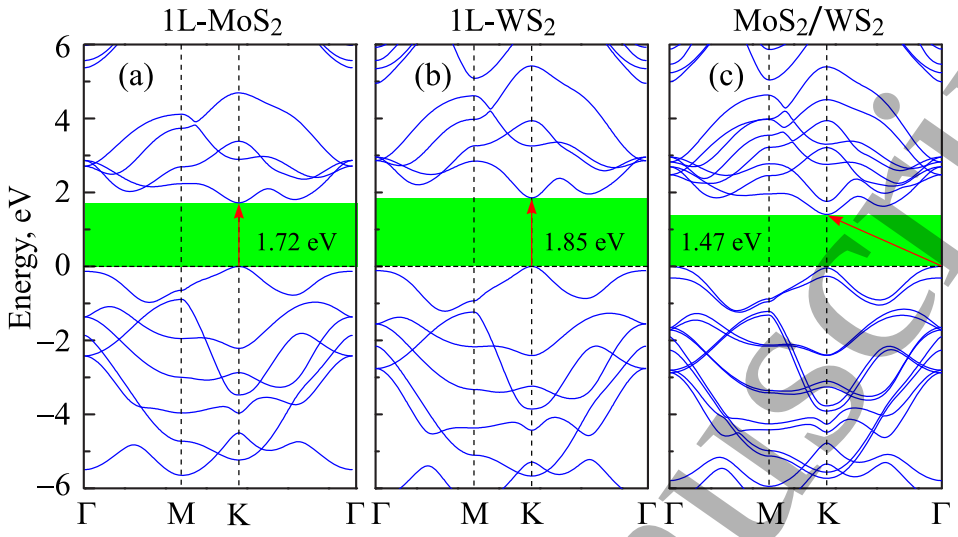

Figure 12. Band structures of the MoS_2 monolayer (a), WS_2 monolayer (b), and MoS_2/WS_2 heterostructure (c).

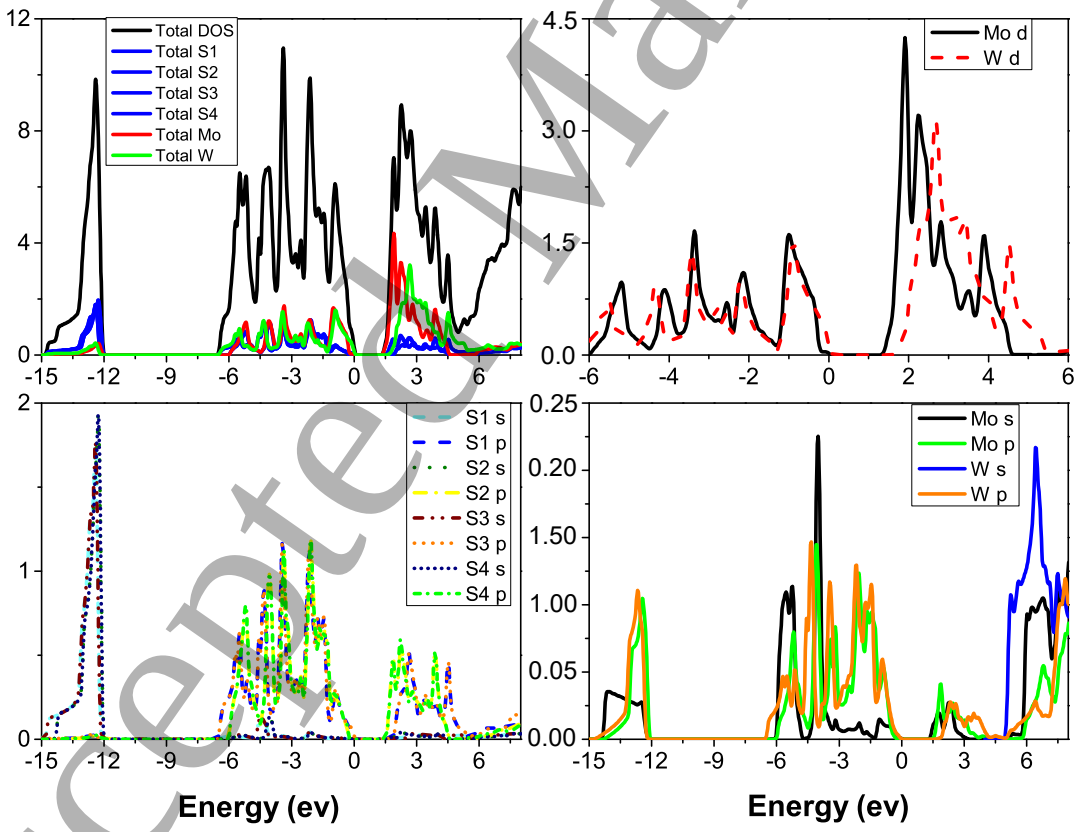

Figure 13. Total and partial densities of states of the vdW MoS_2/WS_2 heterostructure.

for a polarization perpendicular and parallel to the z-axis in the energy range from 0 to 10 eV for the MoS_2 and WS_2 monolayer and their vdW heterostructure. The relative dielectric function of the MS_2 monolayer and their vdW heterostructure is also shown in Fig. 15. The spectra show a similar trend, with the exception of their energy values, it can be seen that

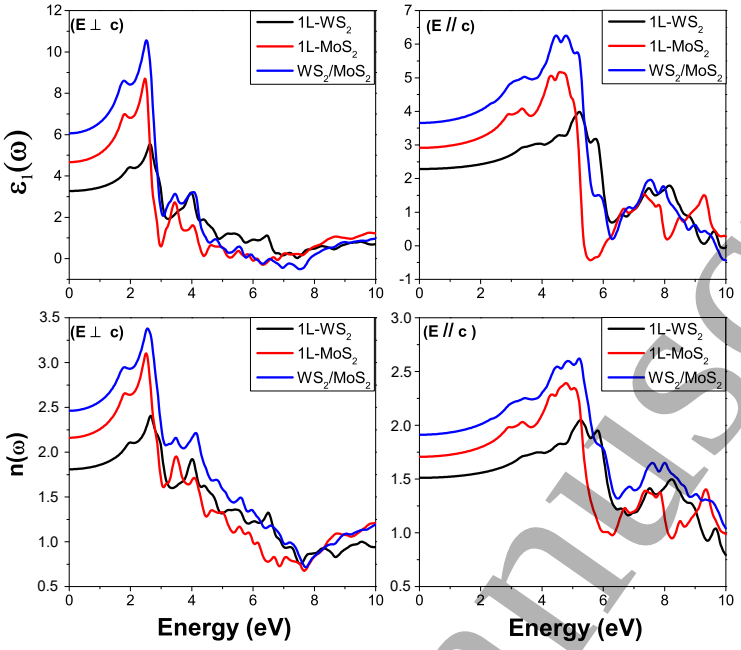

Figure 14. Real dielectric constants $\varepsilon_1(\omega)$ and refraction index $n(\omega)$ of the MoS_2, WS_2 monolayers and MoS_2/WS_2 heterojunction.

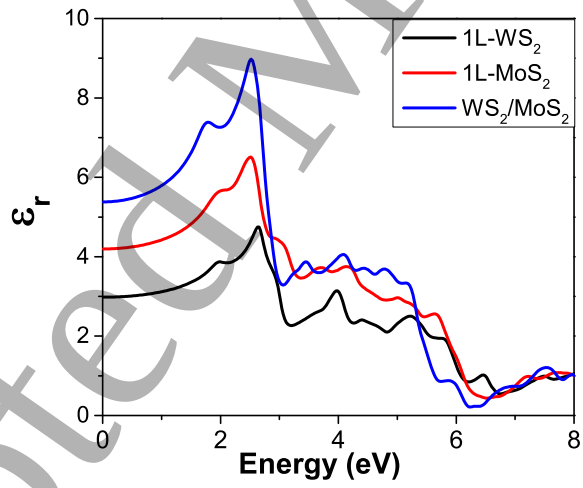

Figure 15. Relative dielectric function of 1L-MoS_2, 1L-WS_2 and MoS_2/WS_2 heterostructure.

the static refractive index, the real dielectric static component and relative dielectric function of the heterostructure are higher than that of WS_2 monolayer. This is a consequence of the decrease in the energy gap.

4. Conclusions

In conclusion, we have systematically investigated the electronic and optical properties of the few-layers MoS_2 and WS_2 and their heterostructure MoS_2/WS_2 using DFT calculations. Quantum confinement (due to reduced material thickness) leads to significantly changes in the

energy structure of the MS_2 (M = Mo, W). Besides, the anisotropy and optical spectrum of the MoS_2 and WS_2 also depend strongly on the number of layers. Whereas the MoS_2 and WS_2 monolayers have a direct band gap, the heterostructure formed by vertical stacking of these monolayers has an indirect band gap. Also, charge carriers in the MoS_2/WS_2 heterostructure are widely localized on different layers and an out-of-plane p-n junction is formed. A type II bands alignment has been formed in the MoS_2/WS_2 bilayer heterostructure which can be advantageous by separating the electron-hole pairs leading to a long lifetime of interlayer excitons. These properties may be useful for applications in nanoelectronic technology.

Acknowledgments

This research is funded by the Vietnam National Foundation for Science and Technology Development (NAFOSTED) under Grant Number 103.01-2017.309. CAD is grateful to the Colombian Agencies CODI-Universidad de Antioquia (Estrategia de Sostenibilidad de la Universidad de Antioquia and project "Efectos de capas delta dopadas en pozos cuánticos como fotodetectores en el infrarrojo") and Facultad de Ciencias Exactas y Naturales-Universidad de Antioquia (CAD exclusive dedication project 2017-2018).

References

[1] Novoselov K S, Geim A K, Morozov S V, Jiang D, Zhang Y, Dubonos S V, Grigorieva I V and Firsov A A 2004 *Science* **306** 666
[2] Nourbakhsh A, Zubair A, Sajjad R N, Tavakkoli K G A, Chen W, Fang S, Ling X, Kong J, Dresselhaus M S, Kaxiras E, Berggren K K, Antoniadis D and Palacios T 2016 *Nano Lett.* **16** 7798
[3] Lalmi B, Oughaddou H, Enriquez H, Kara A, Vizzini S, Ealet B and Aufray B 2010 *Appl. Phys. Lett.* **97** 223109
[4] Lee Y H, Zhang X Q, Zhang W, Chang M T, Lin C T, Chang K D, Yu Y C, Wang J T W, Chang C S, Li L J and Lin T W 2012 *Adv. Mater.* **24** 2320
[5] Novoselov K S, Jiang D, Schedin F, Booth T J, Khotkevich V V, Morozov S V and Geim A K 2005 *Proc. Natl. Acad. Sci. U.S.A* **102** 10451
[6] Coleman J N, Lotya M, O'Neill A, Bergin S D, King P J, Khan U, Young K, Gaucher A, De S, Smith R J, Shvets I V, Arora S K, Stanton G, Kim H Y, Lee K, Kim G T, Duesberg G S, Hallam T, Boland J J, Wang J J, Donegan J F, Grunlan J C, Moriarty G, Shmeliov A, Nicholls R J, Perkins J M, Grieveson E M, Theuwissen K, McComb D W, Nellist P D and Nicolosi V 2011 *Science* **331** 568
[7] Bosi M 2015 *RSC Adv.* **5** 75500
[8] Wickramaratne D, Zahid F and Lake R K 2014 *J. Chem. Phys.* **140** 124710
[9] Bhunia H and Pal A J 2018 *J. Phys. D: Appl. Phys.* **51** 215102
[10] Bernardi M, Palummo M and Grossman J C 2013 *Nano Lett.* **13** 3664
[11] Radisavljevic B, Radenovic A, Brivio J, Giacometti V and Kis A 2011 *Nat. Nanotechnol.* **6** 147
[12] Pu J, Yomogida Y, Liu K K, Li L J, Iwasa Y and Takenobu T 2012 *Nano Lett.* **12** 4013
[13] Wang Q H, Kalantar-Zadeh K, Kis A, Coleman J N and Strano M S 2012 *Nat. Nanotechnol.* **7** 699
[14] Lopez-Sanchez O, Lembke D, Kayci M, Radenovic A and Kis A 2013 *Nat. Nanotechnol.* **8** 497
[15] Xiang R, Hou B, Einarsson E, Zhao P, Harish S, Morimoto K, Miyauchi Y, Chiashi S, Tang Z and Maruyama S 2013 *ACS Nano* **7** 3095
[16] Gong Y, Lin J, Wang X, Shi G, Lei S, Lin Z, Zou X, Ye G, Vajtai R, Yakobson B I, Terrones H, Terrones M, Tay B K, Lou J, Pantelides S T, Liu Z, Zhou W and Ajayan P M 2014 *Nat. Mater.* **13** 1135
[17] Mei J, Li Y T, Zhang H, Xiao M M, Ning Y, Zhang Z Y and Zhang G J 2018 *Biosens. Bioelectron.* **110** 71

[18] Jing Y, Tan X, Zhou Z and Shen P 2014 *J. Mater. Chem. A* **2** 16892
[19] Nguyen C V, Hieu N N, Poklonski N A, Ilyasov V V, Dinh L, Phong T C, Tung L V and Phuc H V 2017 *Phys. Rev. B* **96** 125411
[20] Nguyen C V, Hieu N N, Muoi D, Duque C A, Feddi E, Nguyen H V, Phuong L T T, Hoi B D and Phuc H V 2018 *J. Appl. Phys.* **123** 034301
[21] Liu G B, Shan W Y, Yao Y, Yao W and Xiao D 2013 *Phys. Rev. B* **88** 085433
[22] Cappelluti E, Roldán R, Silva-Guillén J A, Ordejón P and Guinea F 2013 *Phys. Rev. B* **88** 075409
[23] Hieu N N, Ilyasov V V, Vu T V, Poklonski N A, Phuc H V, Phuong L T T, Hoi B D and Nguyen C V 2018 *Superlattices Microstruct.* **115** 10
[24] Geim A K and Grigorieva I V 2013 *Nature* **499** 419
[25] Novoselov K S, Mishchenko A, Carvalho A and Castro Neto A H 2016 *Science* **353** aac9439
[26] Hong X, Kim J, Shi S F, Zhang Y, Jin C, Sun Y, Tongay S, Wu J, Zhang Y and Wang F 2014 *Nat. Nanotechnol.* **9** 682
[27] Lopez-Sanchez O, Lembke D, Kayci M, Radenovic A and Kis A 2013 *Nat. Nanotechnol.* **8** 497
[28] Hieu N N, Phuc H V, Ilyasov V V, Chien N D, Poklonski N A, Hieu N V and Nguyen C V 2017 *J. Appl. Phys.* **122** 104301
[29] Din H U, Idrees M, Rehman G, Nguyen C V, Gan L Y, Ahmad I, Maqbool M and Amin B 2018 *Phys. Chem. Chem. Phys.* **20** 24168
[30] Pham K D, Phuc H V, Hieu N N, Hoi B D and Nguyen C V 2018 *AIP Adv.* **8** 075207
[31] Sun M, Chou J P, Yu J and Tang W 2017 *J. Mater. Chem. C* **5** 10383
[32] Nguyen C V 2018 *Superlattices Microstruct.* **116** 79
[33] Wang S, Ren C, Tian H, Yu J and Sun M 2018 *Phys. Chem. Chem. Phys.* **20** 13394
[34] Phuc H V, Hieu N N, Hoi B D, Phuong L T and Nguyen C V 2018 *Surf. Sci.* **668** 23
[35] Blaha P, Schwarz K, Madsen G, Kvasnicka D and Luitz J 2001 *WIEN2k: An Augmented Plane Wave Plus Local Orbitals Program for Calculating Crystal Properties* (Austria: Vienna University of Technology)
[36] Susarla S, Manimunda P, Morais Jaques Y, Hachtel J A, Idrobo J C, Syed Amnulla S A, Galvão D S, Tiwary C S and Ajayan P M 2018 *ACS Nano* **12** 4036
[37] Mak K F, Lee C, Hone J, Shan J and Heinz T F 2010 *Phys. Rev. Lett.* **105** 136805
[38] Ding Y, Wang Y, Ni J, Shi L, Shi S and Tang W 2011 *Physica B: Conden. Matter* **406** 2254
[39] Gusakova J, Wang X, Shiau L L, Krivosheeva A, Shaposhnikov V, Borisenko V, Gusakov V and Tay B K 2017 *Phys. Status Solidi A* **214** 1700218
[40] Kumar A and Ahluwalia P 2012 *Mater. Chem. Phys.* **135** 755
[41] Yakovkin I N 2014 *Surf. Rev. Lett.* **21** 1450039
[42] Zibouche N, Kuc A, Musfeldt J and Heine T 2014 *Annalen der Physik* **526** 395
[43] Datta K and Khosru D M 2016 *ECS J. Solid State Sci. Technol.* **5** Q3001
[44] López-Suárez M, Neri I and Rurali R 2016 *J. Appl. Phys.* **119** 165105
[45] Ramasubramaniam A 2012 *Phys. Rev. B* **86** 115409
[46] Miwa J A, Ulstrup S, Sørensen S G, Dendzik M, Čabo A G, Bianchi M, Lauritsen J V and Hofmann P 2015 *Phys. Rev. Lett.* **114** 046802
[47] Latzke D W, Zhang W, Suslu A, Chang T R, Lin H, Jeng H T, Tongay S, Wu J, Bansil A and Lanzara A 2015 *Phys. Rev. B* **91** 235202
[48] Schmidt H, Wang S, Chu L, Toh M, Kumar R, Zhao W, Castro Neto A H, Martin J, Adam S, Özyilmaz B and Eda G 2014 *Nano Lett.* **14** 1909
[49] Klein A, Tiefenbacher S, Eyert V, Pettenkofer C and Jaegermann W 2001 *Phys. Rev. B* **64** 205416
[50] Liu G B, Xiao D, Yao Y, Xu X and Yao W 2015 *Chem. Soc. Rev.* **44** 2643
[51] Delin A, Ravindran P, Eriksson O and Wills J M 1998 *Int. J. Quantum Chem.* **69** 349
[52] Reshak A H and Auluck S 2003 *Phys. Rev. B* **68** 125101
[53] Ravindran P, Delin A, Johansson B, Eriksson O and Wills J M 1999 *Phys. Rev. B* **59** 1776
[54] Ravindra N, Ganapathy P and Choi J 2007 *Infrared Phys. Technol.* **50** 21
[55] Beal A R and Hughes H P 1979 *J. Phys. C: Solid State Phys.* **12** 881
[56] Eda G, Yamaguchi H, Voiry D, Fujita T, Chen M and Chhowalla M 2011 *Nano Lett.* **11** 5111

[57] Dashora A, Ahuja U and Venugopalan K 2013 *Comput. Mater. Sci.* **69** 216
[58] Ben Amara I, Ben Salem E and Jaziri S 2016 *J. Appl. Phys.* **120** 051707
[59] Molina-Sánchez A, Hummer K and Wirtz L 2015 *Surf. Sci. Rep.* **70** 554
[60] Sarma S, Mbule P and Ray S C 2019 *Appl. Surf. Sci. [DOI:10.1016/j.apsusc.2019.02.165]*
[61] Goel N, Kumar R, Roul B, Kumar M and Krupanidhi S B 2018 *J. Phys. D: Appl. Phys.* **51** 374003
[62] Dashora A, Ahuja U and Venugopalan K 2013 *Comput. Mater. Sci.* **69** 216
[63] Yang H, Jussila H, Autere A, Komsa H P, Ye G, Chen X, Hasan T and Sun Z 2017 *ACS Photonics* **4** 3023
[64] Aslan O B, Chenet D A, van der Zande A M, Hone J C and Heinz T F 2016 *ACS Photonics* **3** 96
[65] Jalili R, Aminorroaya-Yamini S, Benedetti T M, Aboutalebi S H, Chao Y, Wallace G G and Officer D L 2016 *Nanoscale* **8** 16862
[66] Zhang H, Ma Y, Wan Y, Rong X, Xie Z, Wang W and Dai L 2015 *Sci. Rep.* **5** 8440
[67] Ben Amara I, Ben Salem E and Jaziri S 2017 *Superlattices Microstruct.* **109** 897
[68] Li W, Wang T, Dai X, Wang X, Zhai C, Ma Y, Chang S and Tang Y 2017 *Solid State Commun.* **250** 9
[69] Rivera P, Schaibley J R, Jones A M, Ross J S, Wu S, Aivazian G, Klement P, Seyler K, Clark G, Ghimire N J, Yan J, Mandrus D G, Yao W and Xu X 2015 *Nat. Commun.* **6** 6242
[70] Bellus M Z, Ceballos F, Chiu H Y and Zhao H 2015 *ACS Nano* **9** 6459
[71] Ceballos F, Bellus M Z, Chiu H Y and Zhao H 2015 *Nanoscale* **7** 17523
[72] Rivera P, Yao W and Xu X 2017 Optical properties of tmd heterostructures *2D Materials: Properties and Devices* ed Avouris P, Low T and Heinz T F (Cambridge: Cambridge University Press) pp 310–328.